Short Papers

Experimental Comparison of Position Tracking Control Algorithms for Pneumatic Cylinder Actuators

Gary M. Bone and Shu Ning

***Abstract*—Many researchers have investigated pneumatic servo positioning systems due to their numerous advantages: inexpensive, clean, safe, and high ratio of power to weight. However, the compressibility of the working medium, air, and the inherent nonlinearity of the system continue to make achieving accurate position control a challenging problem. In this paper, two control algorithms are designed for the position tracking problem and their experimental performance is compared for a pneumatic cylinder actuator. The first algorithm is sliding-mode control based on a linearized plant model (SMCL) and the second is sliding-mode control based on a nonlinear plant model (SMCN). Extensive experiments using different payloads (1.9, 5.8, and 10.8 kg), vertical and horizontal movements, and move sizes from 3 to 250 mm were conducted. Averaged over 70 experiments with various operating conditions, the tracking error for SMCN was 18% less than with SMCL. For a 5.8-kg payload and a 0.5-Hz 70-mm amplitude, sine wave reference trajectory, the root-mean-square error with SMCN was less than 0.4 mm for both vertical and horizontal motions. This tracking control performance is better than those previously reported for similar systems.**

***Index Terms*—Actuators, pneumatic systems, position control, servosystems, tracking, variable-structure systems.**

I. Introduction

Many researchers have investigated pneumatic servo positioning systems due to their potential as a low-cost, clean, high power-to-weight ratio actuator. The compressibility of the working medium, air, and the large static and Coulomb friction continue to make achieving accurate position control a challenging problem.

Since this paper involves experimental verification, only recent related papers that included experimental results will be reviewed. A control strategy consisting of proportional plus velocity plus acceleration feedback combined with integral action, null offset compensation, and time-delay minimization was designed and tested in [1]. With a 1.7-kg payload, 250-mm moves were accomplished with steady-state errors (SSE) within ± 1 mm and consistent settling times. The tracking errors were not given. Friction compensation strategies using a neural network and using a nonlinear observer were compared in [2]. Their control system also included an inner proportional-integral-derivative (PID) pressure control loop and an outer PID position control loop. For a 2.7-kg payload and a 0.2 Hz, 70-mm amplitude, sine wave trajectory, the best root-mean-square error (RMSE) was 3 mm. In [3], a novel combination of sliding-mode control and PWM was designed and tested. Tracking errors of ± 2 mm were demonstrated for a 0.25-Hz 25-mm amplitude, sine wave trajectory with a 10-kg payload. An effective sliding-mode observer for estimating the chamber pressures and a sliding-mode controller were presented in [4]. Tracking errors within ± 10 mm were achieved for 300-mm S-curve trajectory.

The systems in [1]–[4] were tested only for horizontal movement, and avoided the effect of gravity loading. A sliding-mode controller that employed differential pressure feedback in place of acceleration feedback was presented in [5]. After tuning for a nominal payload of 10 kg, maximum tracking errors of ± 4, ± 6, and ± 8 mm were observed for 4-, 17-, and 30-kg payloads and a vertical, 0.3 m, 3.14 rad/s, cycloidal input. In [6], an adaptive pole placement controller was applied to a vertically oriented actuator with a 4.5-kg payload. With a conventional pneumatic cylinder, the maximum tracking error was ± 8 mm for a 0.04 Hz, 80-mm amplitude, sine wave trajectory. A controller based on a Takagi–Sugeno fuzzy model and gain-scheduling was presented in [7]. Experiments with 3-, 6-, and 9-kg payloads and vertical motions were included. Tracking errors up to 25 mm occurred with 60-mm S-curve trajectories.

Based on their use in the prior literature and their reputation for robust performance, we chose sliding-mode control (SMC) for our system. We present two SMC algorithms with designs based on our system model [8], and compare their experimental performance for vertical and horizontal motion trajectories. We also test their test-to-test repeatability, and their robustness to significant changes in the payload mass.

Manuscript received July 1, 2006; revised October 26, 2006.

G. M. Bone is with the Department of Mechanical Engineering, McMaster University, Hamilton, ON L8S 4L7, Canada (e-mail: gary@mcmaster.ca).

S. Ning is with the Control, Automation, and Electrical Group, HATCH, Mississauga, ON L5K 2R7, Canada (e-mail: sning@hatch.ca).

Digital Object Identifier 10.1109/TMECH.2007.905718

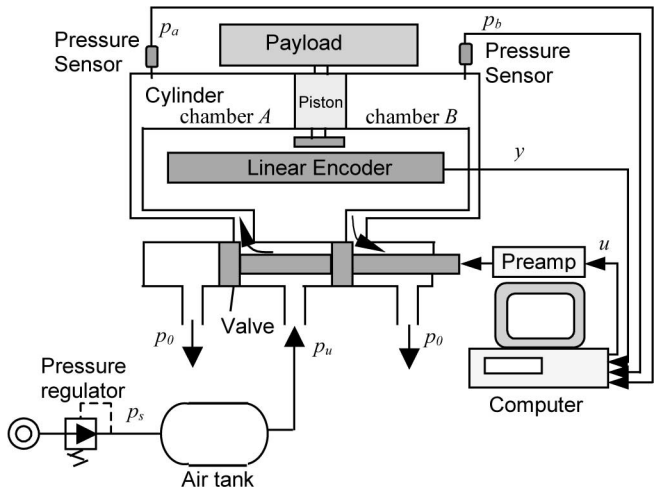

Fig. 1. Pneumatic servo positioning system hardware.

II. System Structure

A schematic diagram of the pneumatic system is shown in Fig. 1. The hardware has been designed to allow the payload mass, type of linear slide, and type of cylinder (e.g., single rod or rodless) to be changed easily. The orientation can also be altered to be vertical or horizontal to change the gravity loading. This flexibility allows testing to be performed over a wide range of conditions. The piston position is measured by a linear incremental encoder with a 0.01-mm resolution. The velocity and acceleration are estimated by digitally differentiating the position signal using backwards differencing. The chamber pressures are measured by two low-cost (U.S. $85) pressure sensors (Omega, model PX139-100D4V). The valve is an open-center proportional type (Festo, model MPYE-5-1/8). The valve, pressure sensors, and encoder are interfaced to a Pentium-based personal computer (PC) that executes the control algorithms. The preamp is used to amplify and bias the signal u from the range ± 2.5 V to the range 0–10-V required for the valve. The PC is programmed in C and a 500-Hz sampling frequency is used.

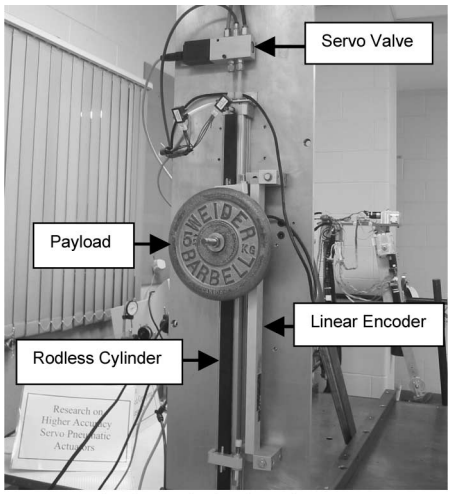

Fig. 2. System set up in the vertical orientation.

A rodless cylinder with 25-mm bore and 600-mm stroke (Festo, model DGPL-25-600) is used for the experiments in this paper. The supply pressure (p_s) was regulated to 0.65 MPa. A photograph of the system set up in the vertical orientation is shown in Fig. 2.

III. Nonlinear System Model

The detailed derivation and parameter estimation of the nonlinear system model were presented in [8] and [9]. The model will only be briefly summarized here. The key equations are

$$\dot{m}_a = f_a(u, p_a) \tag{1}$$

$$\dot{m}_b = f_b(u, p_b) \tag{2}$$

$$KRT\dot{m}_a = Kp_aA_a\dot{y} + A_a(y_{a0} + y)\dot{p}_a \tag{3}$$

$$KRT\dot{m}_b = -Kp_bA_b\dot{y} + A_b(y_{b0} - y)\dot{p}_b \tag{4}$$

$$F_p = (p_aA_a - p_bA_b) + F_l \tag{5}$$

$$F_r = \begin{cases} F_p, & \dot{y} = 0 \text{ and } |F_p| \le F_{\rm sf} \\ F_{\rm sf}, & \dot{y} = 0 \text{ and } |F_p| < F_{\rm sf} \\ F_{\rm cf} + C_{\rm vf}\dot{y}, & \dot{y} > 0 \\ -F_{\rm cf} + C_{\rm vf}\dot{y}, & \dot{y} < 0 \end{cases} \tag{6}$$

$$M\ddot{y} = F_p - F_r \tag{7}$$

where $\dot{m}_a$ and $\dot{m}_b$ are the mass flow rates into the chambers A and B; u is the control signal; K is the specific heat ratio (for air, $K = 1.4$); $R = 287$ J/kg·K is the ideal gas constant; $T = 293$ K is the air temperature; p_a and p_b are the absolute pressures in the chambers A and B; A_a and A_b are the piston areas in the chambers A and B; y is the piston position; y_{a0} is the distance between the piston and the A end of the cylinder when $y = 0$; y_{b0} is the distance between the piston and the B end of the cylinder when $y = 0$; F_p is force on the piston due to the air pressure and the external load F_l; F_r is the total friction force; $F_{\rm sf}$ is the stick-slip friction force; $F_{\rm cf}$ is the Coulomb friction force; $C_{\rm vf}$ is the coefficient of viscous friction; and M is the moving mass (it includes the masses of the payload, slide table, and piston). Based on our previous research, the standard valve nozzle formula was not suitable for modeling the Festo open-center valve. The novel nonlinear functions f_a and f_b in (1) and (2) are detailed in [8]. Note that we did not model the dynamics of the valve's spool. The bandwidth of a proportional valve is usually over 100 Hz (120 Hz for our valve). Since the closed-loop bandwidth of a pneumatic servo is typically not more than 10 Hz, the dynamics of the spool can be neglected without incurring significant modeling error.

IV. Design of Control Algorithms

A. SMC Design Based on Linearized Model

In this section, the design of an SMC algorithm employing a linearized version of our system model as the nominal plant model will be presented. We will denote this algorithm as SMCL. Its design is based on the equivalent control design method from [10]. Applying the standard first-order Taylor series expansion to the system model produced a fourth-order order Laplace transfer function between the piston position and the valve input for a midrange operating point. The dynamics of one transfer function pole and one zero were sufficiently similar to allow their cancellation, resulting in the third-order model (for details, see [9])

$$\dddot{y} = -d_2\ddot{y} - d_1\dot{y} + n_0u. \tag{8}$$

For this plant, a suitable sliding surface is

$$S = \ddot{y} - \ddot{y}_d + 2\lambda(\dot{y} - \dot{y}_d) + \lambda^2(y - y_d). \tag{9}$$

The purpose of the equivalent control signal is to keep the system state on the sliding surface after it has reached it. The state will stay on the surface when $\dot{S} = 0$. The equivalent control signal, $u_{\rm eq}$, is, therefore, obtained by taking the derivative of (9), substituting (8) for $\dddot{y}$, setting $\dot{S} = 0$, and solving for u to give

$$u_{\rm eq} = \left(\dddot{y}_d + d_2\ddot{y} + d_1\dot{y} - 2\lambda(\ddot{y} - \ddot{y}_d) - \lambda^2(\dot{y} - \dot{y}_d)\right)/n_0. \tag{10}$$

To compensate for the system state leaving the sliding surface due to model uncertainty, the switching control signal

$$u_s = -k_s\,\mathrm{sat}(S/\phi) \tag{11}$$

is employed, where $\mathrm{sat}(\cdot)$ is the standard saturation function. The boundary layer thickness ϕ may be tuned to control the amount of chattering of u_s. The total control signal is, then,

$$u = u_{\rm eq} + u_s. \tag{12}$$

The controller parameters ϕ, λ, and k_s will be manually tuned.

B. SMC Design Based on Nonlinear Model

The second SMC design is based on the nonlinear model given by (1)–(7), and will be termed SMCN. It will be more complex to compute than the SMCL, but its use of the nonlinear model should yield better tracking performance.

Substituting (5) into (7), assuming F_l is constant, and differentiating yields

$$M\dddot{y} = \dot{p}_aA_a - \dot{p}_bA_b - \dot{F}_r. \tag{13}$$

Substituting (1) into (3) and (2) into (4), and solving for the pressure derivatives results in

$$\dot{p}_a = \frac{KRTf_a(u, p_a) - Kp_aA_a\dot{y}}{A_a(y_{a0} + y)} \tag{14}$$

and

$$\dot{p}_b = \frac{KRTf_b(u, p_b) + Kp_bA_b\dot{y}}{A_b(y_{b0} - y)}. \tag{15}$$

Since the SMC design allows for model uncertainty, the stick–slip and Coulomb friction components can be neglected in the model such that

$$F_r = C_{\rm vf}\dot{y} \tag{16}$$

and

$$\dot{F}_r = C_{\rm vf}\dddot{y}. \tag{17}$$

Combining (13)–(17) and rearranging gives

$$\dddot{y} = \frac{1}{M}\left(U(u, y, p_a, p_b) - H(y, \dot{y}, p_a, p_b) - C_{\rm vf}\ddot{y}\right) \tag{18}$$

where

$$U(u, y, p_a, p_b) = \frac{KRTf_a(u,\, p_a)}{y_{a0} + y} - \frac{KRTf_b(u,\, p_b)}{y_{b0} - y} \tag{19}$$

and

$$H(y, \dot{y}, p_a, p_b) = \frac{Kp_a A_a \dot{y}}{y_{a0} + y} + \frac{Kp_b A_b \dot{y}}{y_{b0} - y}. \tag{20}$$

Applying the equivalent control design method from [10], with the sliding surface defined by (9) as before, we obtain

$$\dot{S} = \frac{1}{M}\left(U - H - C_{\rm vf}\ddot{y}\right) - \dddot{y}_d + 2\lambda(\ddot{y} - \ddot{y}_d) + \lambda^2(\dot{y} - \dot{y}_d). \tag{21}$$

Setting $\dot{S} = 0$ gives the equivalent control value for U

$$\hat{U}(u_{\rm eq}, y, p_a, p_b) = H(y, \dot{y}, p_a, p_b) + C_{\rm vf}\ddot{y} + M\left(\dddot{y}_d - 2\lambda(\ddot{y} - \ddot{y}_d) - \lambda^2(\dot{y} - \dot{y}_d)\right). \tag{22}$$

Since f_a and f_b are not directly invertible, $\hat{U}$ was solved for $u_{\rm eq}$ by using the measured values of y, p_a, and p_b and linearly interpolating a lookup table. The lookup table was generated offline using (1), (2), and (19). The switching control signal and the total control signal are calculated by (11) and (12). The parameters ϕ, λ, and k_s will be manually tuned.

V. Experimental Verification

A. Procedure

The controllers were designed for the system with a nominal payload mass of 5.8 kg. The corresponding parameters of the nominal linearized model were: $n_0 = 926.8$, $d_1 = 405.8$, and $d_2 = 17.27$. The experimentally determined friction model parameters were: $F_{sf} = 83$ N, $F_{cf} = 34$ N, and $C_{vf} = 78$ N/m/s. For both control algorithms, the manually tuned parameter values were: $\lambda = 70$, $k_s = 0.7$, and $\phi = 4$. These were tuned for the nominal payload mass and horizontal motion. It is important to note that the tuned value of ϕ did not eliminate control signal chatter. In fact, we found that a certain level of chatter acted as a dither signal, reducing the stick-slip friction problem, and improving the tracking performance.

Experiments were performed with two types of reference input trajectories. The first type was a sine wave with a 70-mm amplitude and various frequencies. The second type was a multiple cycloidal trajectory that included four cycloidal motion segments separated by dwell periods. A cycloidal motion segment is similar to an S-curve and is well suited for pneumatic servo systems. Its position, velocity, acceleration, and jerk are given by the equations

$$y_d = -\left(A/\omega^2\right)\sin(\omega t) + (A/\omega)\, t \tag{23}$$

$$\dot{y}_d = -(A/\omega)\cos(\omega t) + A/\omega \tag{24}$$

$$\ddot{y}_d = A\sin(\omega t) \tag{25}$$

and

$$\dddot{y}_d = \omega A\cos(\omega t) \tag{26}$$

TABLE I
Comparison of RMSE (mm) Values for Horizontal Moves With the Nominal Payload (5.8 kg)

	Test 1	Test 2	Test 3	Test 4	Test 5	Mean
0.25 Hz Sine Wave Trajectory						
SMCL	0.364	0.333	0.334	0.338	0.340	0.342
SMCN	0.194	0.190	0.192	0.192	0.185	0.191
0.5 Hz Sine Wave Trajectory						
SMCL	0.358	0.379	0.399	0.404	0.401	0.388
SMCN	0.301	0.283	0.287	0.301	0.306	0.296
1.0 Hz Sine Wave Trajectory						
SMCL	0.776	0.725	0.710	0.825	0.733	0.754
SMCN	0.615	0.606	0.629	0.621	0.641	0.622
Multiple Cycloidal Trajectory						
SMCL	0.312	0.302	0.305	0.357	0.356	0.326
SMCN	0.250	0.225	0.222	0.270	0.204	0.234

where A is the acceleration amplitude, ω is the acceleration frequency, and t is the time. The four motion segments were of sizes 100, 150, −250, and 3 mm. The other parameters for the segments were, respectively: $A = 0.63$ m/s^2, $\omega = 6.3$ rad/s; $A = 0.94$ m/s^2, $\omega = 6.3$ rad/s; $A = -1.38$ m/s^2, $\omega = 6.3$ rad/s; and $A = 0.21$ m/s ^{2} and $\omega = 20.9$ rad/s.

Experiments were conducted with a mismatch between the nominal and actual payload mass to test each of the controller's robustness to modeling errors. Experiments were also conducted with the system in the vertical orientation to study the effect of gravity loading. Each experiment was repeated five times to gauge the repeatability of the closed-loop performance. In addition to SSE, the RMSE values were calculated using the equation

$$\text{RMSE} = \sqrt{\frac{1}{n}\sum_{i=1}^{n} e_i^2} \tag{27}$$

where i is the current sample number, e_i is the error for the current sample, and n is the total number of samples.

B. Experimental Results and Discussion

The RMSE values for the two controllers with no mismatch between the nominal and actual payload masses, and horizontal motion, are listed in Table I. For the same controller and reference input, the maximum deviation from the mean value over the five tests was 0.12 mm, suggesting that the control performance was quite repeatable. The test-to-test variation was probably due to variations in the friction force since the supply pressure was well regulated. The tracking performance worsened as the sine wave frequency increased, mainly due to saturation of the valve input signal. SMCN reduced the RMSE values by 26% on average compared with SMCL.

The effects of a mismatch between the nominal and actual payload masses for horizontal motion are documented in Tables II and III. Surprisingly, when the actual mass was greater than the nominal mass (i.e., 10.8 kg versus 5.8 kg), there was a slight improvement in the tracking performance of the SMCL controller (see Table II). However, the average RMSE values for SMCN worsened by 157% under same conditions. When the actual mass was less than the nominal mass (i.e., 1.9 kg vs. 5.8 kg) the average RMSE value for SMCL increased by 136% relative to the no mismatch case. For SMCN, the increase was only 10%.

TABLE II
COMPARISON OF RMSE (mm) VALUES FOR HORIZONTAL MOVES WITH A PAYLOAD OF 10.8 kg (i.e., 86% MORE THAN NOMINAL)

	Test 1	Test 2	Test 3	Test 4	Test 5	Mean
0.5 Hz Sine Wave Trajectory						
SMCL	0.366	0.352	0.408	0.378	0.372	0.375
SMCN	0.720	0.725	0.770	0.717	0.650	0.716
Multiple Cycloidal Trajectory						
SMCL	0.259	0.203	0.217	0.193	0.194	0.213
SMCN	0.550	0.591	0.780	0.696	0.624	0.648

TABLE III
COMPARISON OF RMSE (mm) VALUES FOR HORIZONTAL MOVES WITH A PAYLOAD OF 1.9 kg (i.e., 67% LESS THAN NOMINAL)

	Test 1	Test 2	Test 3	Test 4	Test 5	Mean
0.5 Hz Sine Wave Trajectory						
SMCL	0.989	1.01	1.04	0.984	1.086	1.022
SMCN	0.326	0.325	0.331	0.327	0.318	0.325
Multiple Cycloidal Trajectory						
SMCL	0.682	0.668	0.653	0.674	0.644	0.664
SMCN	0.240	0.233	0.271	0.261	0.280	0.257

TABLE IV
COMPARISON OF RMSE (mm) VALUES FOR VERTICAL MOVES WITH THE NOMINAL PAYLOAD (5.8 kg)

	Test 1	Test 2	Test 3	Test 4	Test 5	Mean
0.5 Hz Sine Wave Trajectory						
SMCL	0.301	0.324	0.313	0.311	0.334	0.317
SMCN	0.277	0.305	0.269	0.253	0.262	0.273
Multiple Cycloidal Trajectory						
SMCL	0.239	0.234	0.237	0.204	0.191	0.221
SMCN	0.322	0.361	0.314	0.357	0.396	0.350

The tracking results when moving in the vertical direction with no mismatch between the nominal and actual payloads are given in Table IV. Compared to the horizontal orientation, the average RMSE values for the 0.5-Hz sine wave trajectory improved by 18% and 8% for SMCL and SMCN, respectively. With the multiple cycloidal trajectory, the SMCL performance improved, while the SMCN results worsened. It was expected that the gravity loading would worsen the performance of both the controllers. It was later found that the friction force from the linear slide reduced when it was in the vertical orientation. The odd pattern of behavior was the result of the lowered friction force being more influential than the added gravity loading. This conclusion was supported by a simulation study.

In Tables V and VI, the tracking results for vertical moves with mismatches between the nominal and actual payloads are presented. When the actual mass was greater than the nominal mass, the average RMSE values increased by 44% and 133% relative to the values for no mismatch for SMCL and SMCN, respectively (see Tables IV and V). When the mass was less than the nominal value, for SMCL, an increase of 217% occurred, while, for SMCN, a decrease of 23% occurred (see Tables IV and VI).

From these results, we can conclude that SMCL is more robust than SMCN when the actual payload is greater than the nominal value, while SMCN is more robust when the actual payload is less than the nominal

TABLE V
COMPARISON OF RMSE (mm) VALUES FOR VERTICAL MOVES WITH A PAYLOAD OF 10.8 kg (i.e., 86% MORE THAN NOMINAL)

	Test 1	Test 2	Test 3	Test 4	Test 5	Mean
0.5 Hz Sine Wave Trajectory						
SMCL	0.336	0.428	0.332	0.365	0.354	0.363
SMCN	0.884	0.751	0.799	0.828	0.791	0.810
Multiple Cycloidal Trajectory						
SMCL	0.471	0.414	0.384	0.352	0.432	0.411
SMCN	0.602	0.713	0.606	0.696	0.599	0.643

TABLE VI
COMPARISON OF RMSE (mm) VALUES FOR VERTICAL MOVES WITH A PAYLOAD OF 1.9 kg (i.e., 67% LESS THAN NOMINAL)

	Test 1	Test 2	Test 3	Test 4	Test 5	Mean
0.5 Hz Sine Wave Trajectory						
SMCL	1.01	0.987	1.01	0.989	0.998	0.999
SMCN	0.267	0.254	0.268	0.267	0.280	0.267
Multiple Cycloidal Trajectory						
SMCL	0.936	0.641	0.642	0.659	0.648	0.705
SMCN	0.210	0.212	0.216	0.200	0.226	0.213

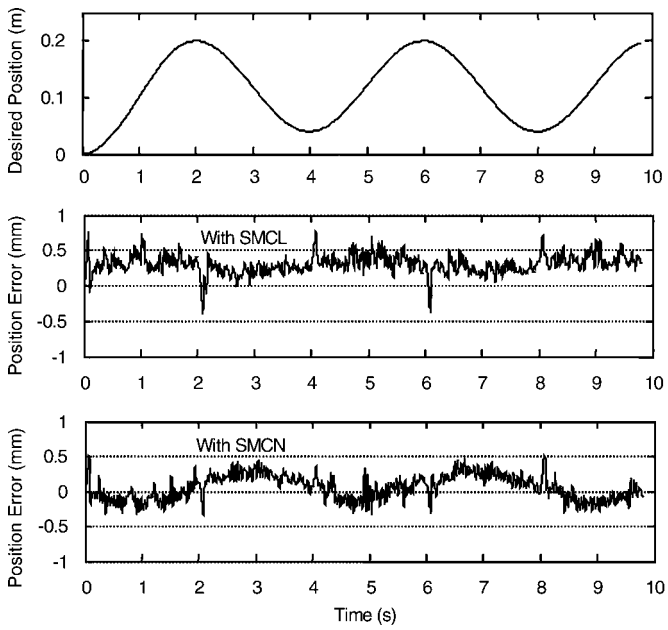

Fig. 3. Experimental results for a horizontal 0.25-Hz 70-mm amplitude, sine wave trajectory, and a 5.8-kg payload controlled using SMCL (middle) and SMCN (bottom).

value. The tracking performance obtained with SMCN was slightly superior to that with SMCL. Averaged over the 70 tests performed with each algorithm, the RMSE was 0.51 mm for SMCL, and, for SMCN, it was 0.42 mm.

Two experimental results for a 0.25 Hz, 70-mm amplitude, horizontal sine wave trajectory are plotted in Fig. 3. The tracking errors for SMCL and SMCN were less than ± 0.75 mm and ± 0.5 mm, respectively.

Results for a vertical multiple cycloidal trajectory and a 10.8-kg payload (with no mismatch) are plotted in Fig. 4. For both the algorithms, the tracking errors stayed within ± 1.3 mm. The SSE

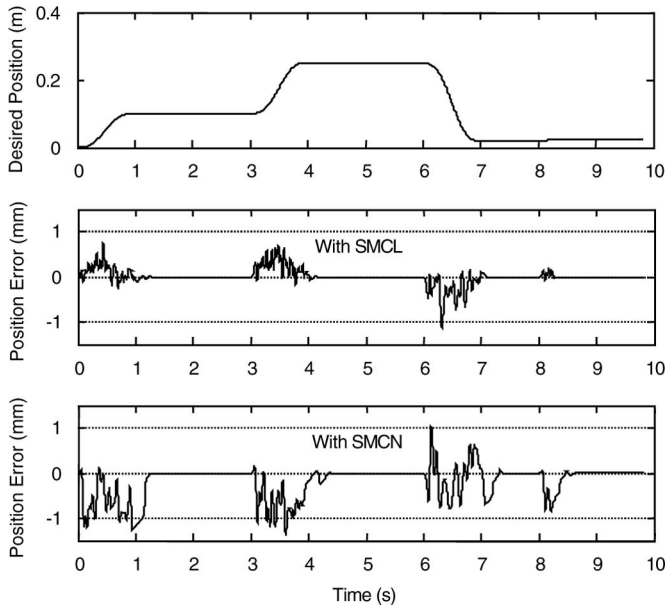

Fig. 4. Experimental results for a vertical multiple cycloidal trajectory and a 10.8-kg payload controlled using SMCL (middle) and SMCN (bottom).

did not exceed ± 0.01 mm. This level of steady-state performance was achieved in all of the horizontal and vertical multiple cycloidal tests performed.

VI. Conclusion

Two model-based sliding-mode position tracking control algorithms for pneumatic cylinder actuators were designed and extensively tested. Such a comparison study has not appeared in the previous literature. The tests demonstrated that both controllers were effective at tracking multiple cycloidal and sine wave reference trajectories in horizontal and vertical orientations. It was found that gravity loading did not have a significant adverse effect on the transient or steady-state performance. This is likely due to gravity acting as a constant disturbance. The SSE did not exceed ± 0.01 mm. The tracking performance for SMCL was more greatly affected by the payload mass being less than the nominal value, than it was by the mass being greater than the nominal value. The opposite was true for the SMCN. For SMCN, the RMSE value averaged over the full range of tests performed was 0.42 mm. For SMCL, the value was 0.51 mm. Depending on the application, the level of performance improvement obtained with SMCN may not warrant its added complexity and requirement for pressure sensors.

The tracking performances of both the control algorithms are better than those reported in the prior literature for similar pneumatic servo systems and test conditions.

References

[1] J. Wang, J. Pu, and P. Moore, "A practical control strategy for servo-pneumatic actuator systems," *Control Eng. Pract.*, vol. 7, pp. 1483–1488, 1999.

[2] H. K. Lee, G. S. Choi, and G. H. Choi, "A study on tracking control of pneumatic actuators," *Mechatronics*, vol. 12, pp. 813–831, 2002.

[3] E. J. Barth, J. Zhang, and M. Goldfarb, "Sliding mode approach to PWM-controlled pneumatic systems," in *Proc. 2002 Amer. Control Conf.*, pp. 2362–2367.

[4] S. R. Pandian, F. Takemura, Y. Hayakawa, and S. Hayakawa, "Pressure observer-controller design for pneumatic cylinder actuators," *IEEE/ASME Trans. Mechatronics*, vol. 7, no. 4, pp. 490–499, Dec. 2002.

[5] S. R. Pandian, Y. Hayakawa, Y. Kanazawa, Y. Kamoyama, and S. Kawamura, "Practical design of a sliding mode controller for pneumatic actuators," *Trans. ASME, J. Dyn. Syst. Meas. Control*, vol. 119, pp. 666–674, 1997.

[6] R. Richardson, A. R. Plummer, and M. D. Brown, "Self-tuning control of a low-friction pneumatic actuator under the influence of gravity," *IEEE Trans. Control Syst. Technol.*, vol. 9, no. 2, pp. 330–334, Mar. 2001.

[7] H. Schulte and H. Hahn, "Fuzzy state feedback gain scheduling control of servo-pneumatic actuators," *Control Eng. Pract.*, vol. 12, pp. 639–650, 2004.

[8] S. Ning and G. M. Bone, "Development of a nonlinear dynamic model for a servo pneumatic positioning system," in *Proc. IEEE Int. Conf. Mechatronics Autom.*, 2005, pp. 43–48.

[9] S. Ning "Theoretical and experimental study of pneumatic servo motion control systems," Ph.D. dissertation, Mech. Eng. Dept., McMaster Univ., Hamilton, ON, Canada, 2004.

[10] J. Slotine and W. Li, *Applied Nonlinear Control*. Englewood Cliffs, NJ: Prentice-Hall, 1991, ch. 7.

Industrial Applications of Online Machining Process Monitoring System

Dongfeng Shi and Nabil N. Gindy

***Abstract*—An online machining process monitoring system has been constructed by taking advantage of the new achievements in data acquisition, sensor technology, and signal processing. Firstly, the architecture of monitoring system with the capability of automatic online acquisition, presentation, and analysis sensory signals is designed. Secondly, wavelet transform is further explored to decompose sensory signals into static and dynamic components for the purpose of extracting distinctive features associated with different tool malfunctions. Thirdly, by conjunction with the wavelet transform, univariate and multivariate statistical process monitoring techniques are proposed to construct the thresholds of malfunction-free machining zone. Short time Fourier transform is further introduced to detect the onset of chattering in machining processes. Finally, the effectiveness of the developed techniques and monitoring system has been demonstrated by experimental results obtained from the extensive industrial machining trials.**

***Index Terms*—Process monitoring, signal processing, statistical process control, wavelet transform.**

I. Introduction

Although poor finishing quality due to tool malfunctions may be inspected by time-consuming nondestructive inspection, the development of online machining process monitoring has received more and more attention to reduce production losses and improve product quality

Manuscript received October 16, 2006; revised February 14, 2007. Recommended by Technical Editor J. R. Wagner. This work was supported by the British Engineering and Physical Sciences Research Council.

D. Shi is with the School of Aerospace Engineering, Nanjing University of Aeronautics and Astronautics, Nanjing 210016, China (e-mail: dongfeng.shi@gmail.com).

N. N. Gindy is with the School of Mechanical, Materials and Manufacturing Engineering, University of Nottingham, Nottingham NG7 2RD, U.K. (e-mail: nabil@nottingham.ac.uk).

Color versions of one or more of the figures in this paper are available online at http://ieeexplore.ieee.org.

Digital Object Identifier 10.1109/TMECH.2007.902131